22nd International Congress on Instrumentation in Aerospace Simulation Facilities
10-14 June, 2007, Pacific Grove, California
SAND2007-3311C

A Combined PIV / Force Balance Study of a Fin-Wake Aerodynamic Interaction

Steven J. Beresh, Justin A. Smith, John F. Henfling, Thomas W. Grasser, and Russell W. Spillers

Sandia National Laboratories
PO Box 5800, Mailstop 0834, Albuquerque, NM, 87111, USA
Email: sjberes@sandia.gov

A sub-scale experiment has been constructed using fins mounted on one wall of a transonic wind tunnel to investigate the influence of fin tip vortices upon downstream control surfaces. Data are collected using a fin balance mounted on the downstream fin to measure the aerodynamic forces of the interaction, combined with stereoscopic Particle Image Velocimetry to measure vortex properties. The fin balance data show that the response of the downstream fin essentially is shifted from the baseline single-fin data dependent upon the angle of attack of the upstream fin. Freestream Mach number and the spacing between fins have secondary effects. The velocimetry shows that the vortex strength increases markedly with upstream fin angle of attack, though even an uncanted fin generates a noticeable wake. No Mach number effect can be discerned in the normalized data, but data taken progressively further from the fin trailing edge show the decay in vortex strength with downstream distance. Correlations between the force data and the velocimetry suggest that the interaction is fundamentally a result of an angle of attack induced upon the downstream fin by the vortex shed from the upstream fin tip.

Introduction

As a result of the precision-guidance capabilities found on many modern missiles and bombs, the complexity of the aerodynamic control surfaces is increasing as many vehicles now combine the presence of fins with strakes or canards. Consequently, the tip vortices shed from the upstream control surfaces propagate downstream where they can interact with those downstream and dramatically alter the expected performance, an interaction for which neither the knowledge base nor the predictive modeling is adequately developed. The severity of this interaction can be extreme, sometimes leading to an inability to control the vehicle at all, much less with the great precision for which it was intended.

Such fin-wake interactions often are addressed by conducting wind tunnel tests on specific flight configurations, then deriving aerodynamic models that can be used by the guidance system. Clearly, this approach is inefficient due to the need for new data following every design change in order to assure an accurate aerodynamic model, and the use of reliable predictive tools to minimize the testing requirements is greatly preferable. While a number of engineering-level predictive methods exist (for example, [1,2]), they are hampered by the difficult challenge of accurately predicting the vortices shed by control surfaces across a wide range of flow conditions and geometric variations. Higher-fidelity CFD predictions may be attempted, but generate considerable computational expense as well as questions regarding the accuracy of their results. Regardless of the computational tool, it must be validated against reliable experimental data for the regime in which it will be applied, but some studies have indicated that common predictive codes, despite some impressive successes, may exhibit significant deficiencies for guided-missile geometries [3-5].

To approach this problem, an experimental program is underway in Sandia's Trisonic Wind Tunnel (TWT) to study the vortex shed from a fin installed on a wall of the tunnel and its impingement upon a second fin placed downstream of the first. The wind tunnel wall represents the surface of a hypothetical flight vehicle rather than employing a traditional sting-mounted model of a missile body, so that a reasonably sized flowfield may be produced in a smaller facility. Data on the structure of the wake of the upstream fin are measured using Particle Image Velocimetry (PIV), coupled with fin force and moment instrumentation using a specialized balance to determine its altered aerodynamic performance. Such a data set can be used to develop and validate computational models within the flight regime of interest to Sandia for precision-guidance flight hardware.

Experimental Apparatus

Trisonic Wind Tunnel

Experiments were performed in Sandia's Trisonic Wind Tunnel (TWT), which is a blowdown-to-atmosphere facility using air as the test gas through a 305 × 305 mm^2 (12 × 12 inch^2) rectangular test section enclosed within a pressurized plenum. Several test section configurations are possible using either porous walls to alleviate the transonic choking condition or solid walls for subsonic compressible conditions. The solid-wall transonic test section was used for the present work rather than the traditional ventilated version because it offers reasonable optical access, a flat plate upon which models may be mounted from the wall, and computationally tractable boundary conditions for comparison of experimental data and numerical simulations. The use of a solid-wall test section limits the Mach number range of the flowfield, but this was considered an acceptable compromise.

Fin Hardware

The data presented in the current report use a single design for both fins, shown in Fig. 1, as a generic representation of the

various fin geometries that could be found on real-world systems. Based upon a trapezoidal planform, the leading edge sweep is 45°, the fin root chord 76.2 mm (3 inch), the fin span 38.1 mm (1.5 inch), and its thickness 3.18 mm (0.125 inch). The sharp leading edge has a taper that terminates at a length of 1/3 the chord. Fins were fabricated from stainless steel to guard against aeroelastic deformation and black oxide coated to reduce background light scatter for the PIV measurements.

Each fin attaches to either the fin balance or a low-profile dummy balance, passing through the test section wall using a hub and pin system. This is shown in Fig. 2 with the downstream fin attached to the balance, which is described below. Both the balance and the dummy balance mount can be set to discrete angles of attack ranging from -5° to +10° in 1° increments, pinned in place to tightly-toleranced positions to promote repeatability. A gap of 1.5 mm (0.06 inch) exists between the root of the fin and the wind tunnel wall.

The axial position of each fin is adjustable within a range of 457 mm (18.0 inch) using a series of interchangeable sliding mounting blocks within a rail cut into the test section wall. Some limitations are placed upon the fin position when connected to the balance due to interference from the tunnel infrastructure behind the wall, but the dummy balance is of sufficiently small stature that it fits anywhere. Repositioning the fins between wind tunnel runs allows an examination of the spacing between fins as an experimental parameter, in combination with adjusting the angles of attack of each fin.

Fin Force Balance

Two customized fin balances were procured from Allied Aerospace's Force Measurement Systems division, differing only in their loading range. Each balance is capable of measuring three components: the fin normal force, the bending moment, and the hinge moment; owing to the relatively thin fin size, the axial force is assumed to be negligible. Only one of the two balances was needed for the present work, providing a maximum load of 220 N (50 lbs-force) normal force. The design is essentially the same as a strain-gage internal balance routinely used in aerodynamic testing. The balance aligns along the fin axis of rotation and is mounted behind the wind tunnel wall, as shown in Fig. 2, using a cylindrical housing. The balance rotates within the canister along with the fin when adjusted to different angles of attack with respect to the oncoming flow. The mechanism to set the fin angle is attached to the rear of the balance and operates as described above.

The balance was calibrated by adapting it to a calibration stand, normally used for calibrating internal balances, and replacing the fin with a calibration plate that allows weights to be hung from 18 different locations. The combination of different loading positions and weight magnitudes could load all three components simultaneously and thus excite interactions between them, allowing a full calibration on a 3 × 9 matrix. Calibration results were shown to agree with the factory calibration to within the expected repeatability of the balance (0.1-0.2% of full-scale measurement).

Particle Image Velocimetry System

The PIV laser sheet configuration for the fin vortex

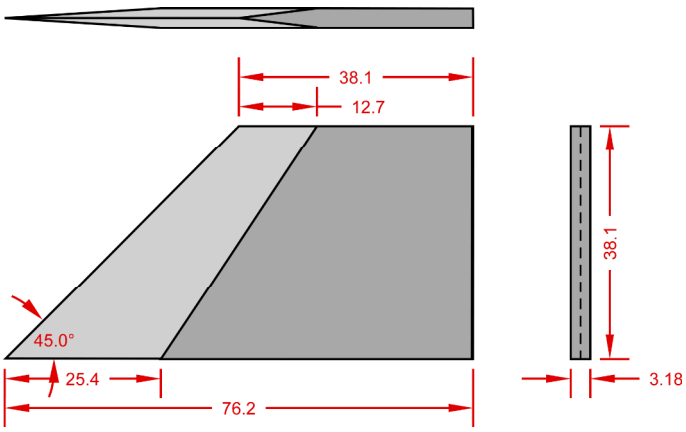

Figure 1: Sketch of the fin geometry. Dimensions in mm.

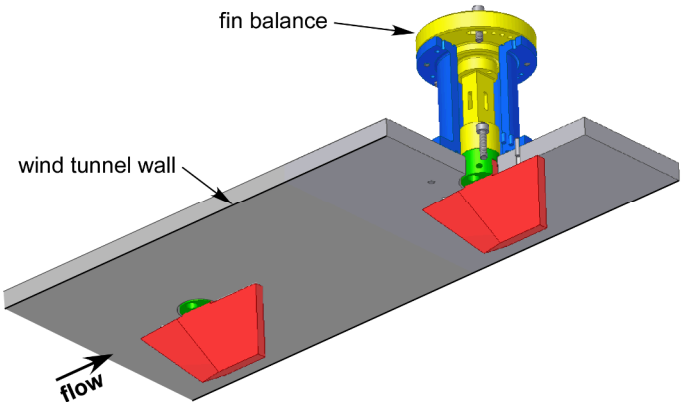

Figure 2: Mounting of fins to the top wall of the test section, where the downstream fin is attached to a fin balance.

measurements in the TWT is shown in Fig. 3, in which stereoscopic PIV is used to obtain all three velocity components in the wind tunnel crossplane. The laser sheet was aligned normal to the wind tunnel axis and positioned to the midpoint of the test section side-wall window. The coordinate system is chosen such that the u component lies in the streamwise direction and the v component is in the vertical direction, positive away from the top wall; the w component is chosen for a right-handed coordinate system. The origin is located at the trailing edge of the fin root, regardless of its position along the test section axis.

The light source was a frequency-doubled dual-cavity Nd:YAG laser (Spectra Physics PIV-400) that produced as much as 400 mJ per beam. The beams were formed into coplanar sheets and directed into the test section from beneath the wind tunnel. To limit the particle dropout arising from the alignment of the freestream direction of the wind tunnel with the out-of-plane motion through the laser sheet, a relatively thick laser sheet of 2.0 mm and brief time between pulses of 1.80 µs were employed.

The TWT is seeded by a thermal smoke generator (Corona Vi-Count 5000) that produces a large quantity of particles typically 0.2 - 0.3 µm in diameter from a mineral oil base. Particles are delivered to the TWT's stagnation chamber upstream of the flow conditioning section and are sufficiently

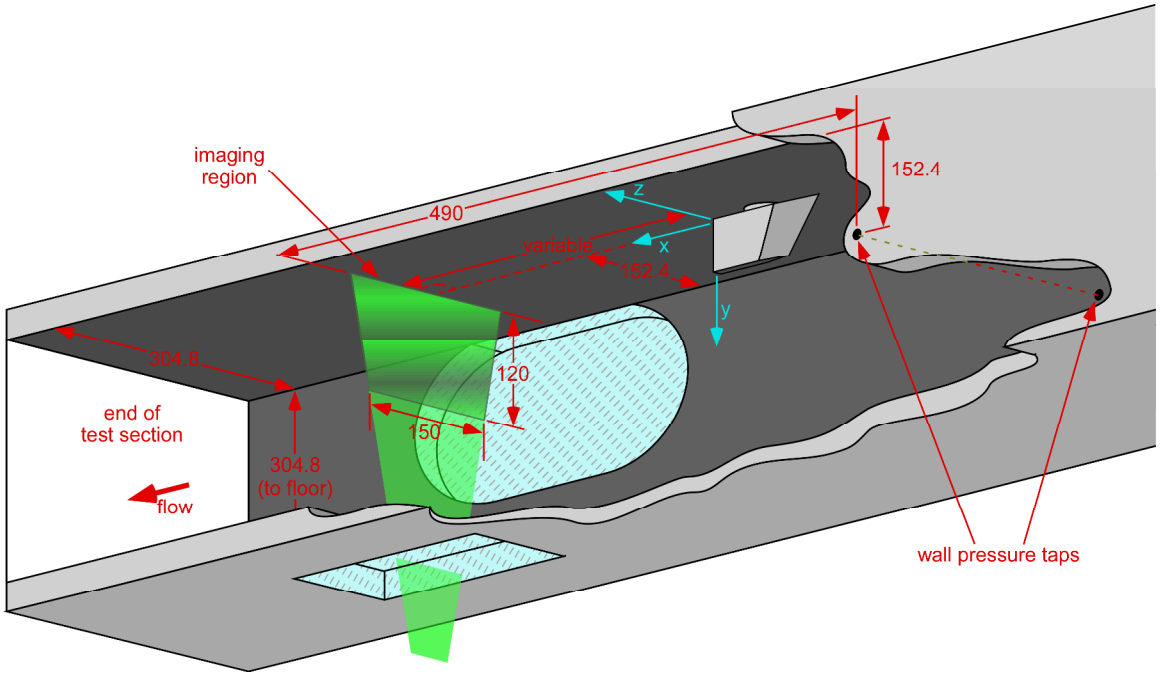

Figure 3: Schematic of the crossplane configuration for PIV measurements, looking in the downstream direction from below the test section. Flow is from right to left. All dimensions are in millimeters. Not to scale.

small that they rapidly attain the local velocity even in the presence of velocity gradients due to the fin tip vortex [6, 7].

Scattered laser light was collected by frame-straddling CCD cameras (Redlake MegaPlus ES4.0/E), which allow the exposure associated with each laser pulse to be stored independently. Each camera has a resolution of 2048 × 2048 pixels digitized at 8 bits and is connected to its own acquisition computer to allow image collection at the maximum rate possible, found to be 5 image pairs per second to maintain synchronization between cameras. Commercially available software was used to control the cameras and computer hardware (SpeedVision OmniSpeed) and timing synchronization between the cameras and laser was accomplished using two digital delay generators (Stanford Research Systems DG535).

The two cameras were equipped with 105 mm lenses (Nikon Micro-Nikkor) mounted on Scheimpflug platforms to create an oblique focal plane aligned with the laser sheet. Both cameras looked through the same test section window, viewing the laser sheet from opposite directions, because placing one camera at the other side-wall window would have precluded access to the test section. To improve upon the limited camera viewing angles due to the constricted optical access through windows originally designed for schlieren imaging, mirrors were rigidly mounted inside the plenum to reflect scattered laser light to the cameras at a sharper angle, as sketched in Fig. 4. This approach allowed an angle of 55° between the camera lenses and the laser sheet normal. The limited optical access additionally prevents meaningful movement of the crossplane location upstream or downstream; thus all data have been acquired at a single position within the test section. Different stations with respect to the fin were achieved by moving the fin's location.

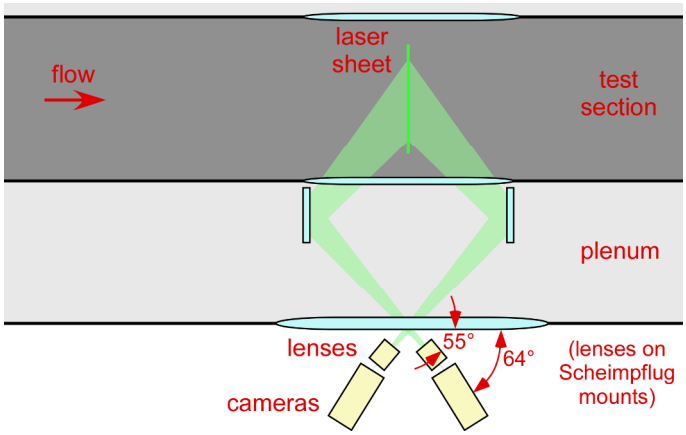

Figure 4: Schematic of the camera arrangement for crossplane stereoscopic PIV in the Trisonic Wind Tunnel.

To calibrate the stereoscopic system, the distorted sheet procedure described by Soloff et al. [8] has been used, alternatively known as the "thick sheet" calibration. An aluminum plate 3.05 mm (0.120 inch) thick and flat to within 0.05 mm (0.002 inch) was fabricated with holes drilled every 12.7 mm (0.500 inch) as fiduciary marks upon which the PIV calibration software can correlate. The calibration target was precisely aligned coplanar to the laser sheet position and translated through the measurement volume while a sequence of images was acquired by each camera. The resulting calibration images were used by the data processing software to tie together the two sets of image pairs to produce three-dimensional vectors.

Data were processed using commercial software (LaVision's

DaVis v7.1). Image pairs were interrogated with a 64 × 64 pixel window employing adaptive correlations and a spatial offset to account for the mean streamwise particle displacement. A 50% overlap in the interrogation windows was used as well to oversample the velocity fields. The resulting vector fields were validated based upon signal-to-noise ratio and nearest-neighbor comparisons. All vector fields shown in the present paper are mean data found from a single wind tunnel run of 150 instantaneous samples.

Experimental Conditions

Testing conditions have been selected to represent a portion of the range flown by transonic vehicles that may incorporate precision guidance capabilities. Limitations of the solid-wall test section restrict the maximum Mach number possible, but future studies will address true transonic flow very near Mach 1. For the present work, the nominal freestream Mach number is M_∞=0.5, 0.6, 0.7, and 0.8 with the wind tunnel stagnation pressure P_0 set to yield a test section static pressure p_w=101 kPa (14.7 psia). The wind tunnel Reynolds number at these conditions is 11×10^6, 13×10^6, 16×10^6, and 19×10^6 m^{-1} (3.3×10^6, 4.0×10^6, 4.9×10^6, and 5.7×10^6 ft^{-1}), respectively. The wind tunnel air supply is heated in the storage tanks, but not temperature-controlled subsequent to this; therefore the freestream stagnation temperature T_0 is subject to minor variation and fluctuates from 316 K to 328 K (108 - 130°F).

The wall pressure p_w was measured from the mean of two static pressure taps located on the wind tunnel side walls 490 mm upstream of the laser sheet location, as seen in Fig. 3. M_∞ and the freestream velocity U_∞ were calculated isentropically from the ratio p_w/P_0 and the stagnation temperature T_0. The freestream Mach number rises with downstream distance due to boundary layer growth on the wind tunnel walls in the constant-area cross-section; hence, the actual Mach number at the fin location or laser sheet position will be greater than the nominal value established for the flow. To determine the local value, a series of pressure taps were installed in one side wall of the test section and recorded during every wind tunnel run. The greatest rise occurs at Mach 0.8, where an increase to Mach 0.834 is observed at the laser sheet position.

The 99%-velocity boundary layer thickness has been measured as 15.4 ± 0.4 mm (0.61 ± 0.02 inch) from PIV data acquired in the streamwise plane [9]. This measurement was made on the wind tunnel centerline at the same downstream position as the crossplane laser sheet.

Results and Discussion

Fin Aerodynamics

Data first were acquired using the fin balance on a single fin to obtain a baseline for fin performance free of aerodynamic interference from an upstream fin. Following this activity, the second fin was placed into the wind tunnel. Initially, the upstream and downstream fins were separated by a length of three fin root chords measured from fin center to fin center. The angle of the upstream fin, α_1, successively was set to four different angles, while the downstream fin angle, α_2, was cycled through different angles as well. The results are shown in Fig. 5 for the normal force coefficient C_{NF}, the bending moment coefficient C_{BM}, and the hinge moment coefficient C_{HM}. Coefficients are normalized by the dynamic pressure at the local Mach number (i.e., accounting for the increase due to boundary layer growth) and the fin planform area; the two moments are additionally normalized by the fin span or the average chord, respectively.

Figure 5 shows the alteration of the forces and moments on the downstream fin due to presence of the vortex shed from the fin tip of the upstream fin. The normal force, C_{NF}, essentially shifts above or below the single-fin data based upon the angle of attack of the upstream fin. In the case of no upstream fin cant, the data do not change significantly from the single-fin case, with slight deviation at the highest angles of attack for the downstream fin. This occurs because no vortex is generated when the upstream fin is aligned with the freestream, though a wake can be expected. As the upstream fin becomes canted, the additional effect of the generated vortex upon the downstream fin becomes evident, which appears to be largely constant across the range of downstream fin angles (this turns out to be accurate except at α_2=10°). Behavior of the bending moment is virtually identical, but the hinge moment displays some convergence of the data at large downstream fin angle.

The effect upon the aerodynamic coefficients due to changing the freestream Mach number is given in Fig. 6. Data

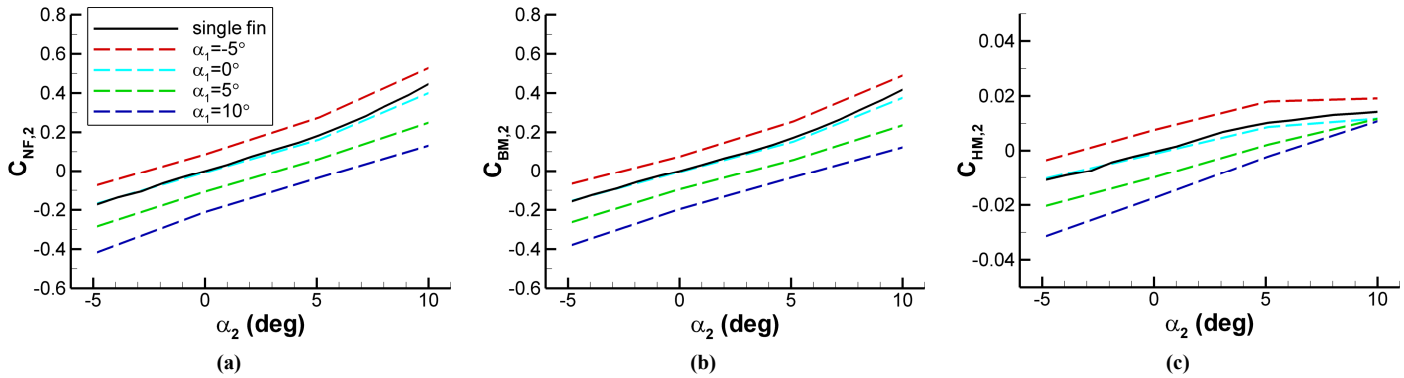

Figure 5: Aerodynamic coefficients of the downstream fin as the upstream fin angle of attack is altered. Single fin data are shown for comparison. (a) normal force; (b) bending moment; (c) hinge moment.

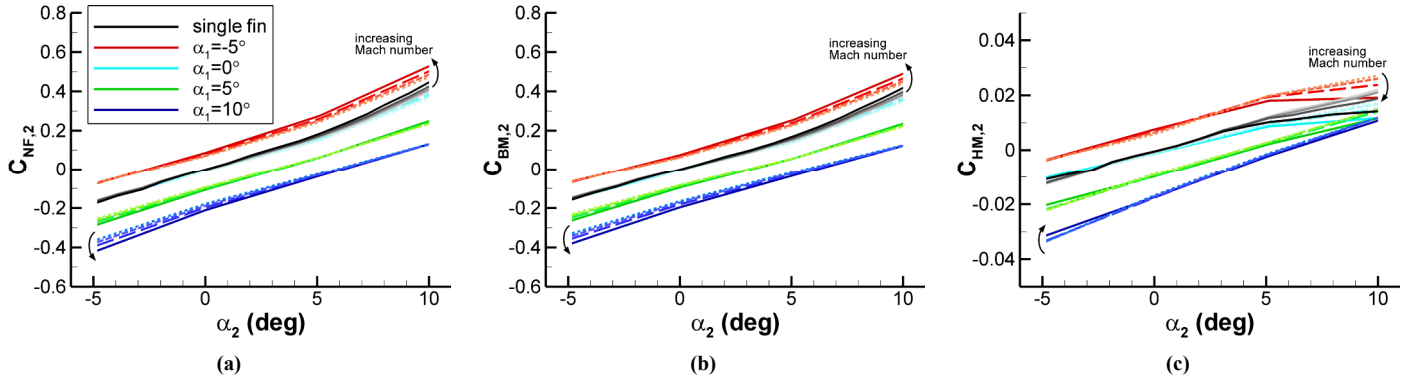

Figure 6: Mach number effect upon the aerodynamic coefficients of the downstream fin, for M_∞=0.5, 0.6, 0.7, and 0.8. Single fin data are shown for comparison. (a) normal force; (b) bending moment; (c) hinge moment.

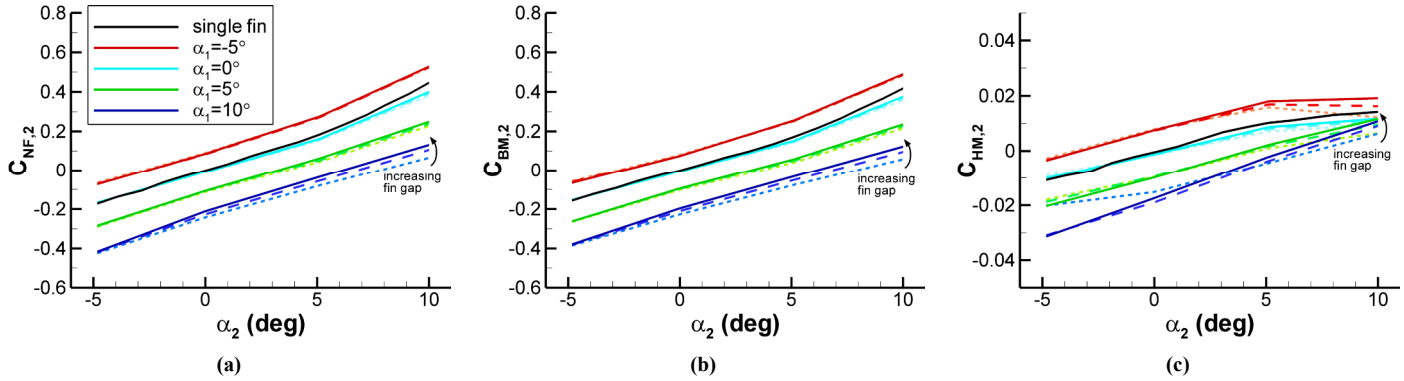

Figure 7: Fin spacing effect upon the aerodynamic coefficients of the downstream fin, for G/c=1, 2, and 3. Single fin data are shown for comparison. (a) normal force; (b) bending moment; (c) hinge moment.

curves are plotted for nominal Mach numbers increasing from M_∞=0.5 to 0.8, where deepening color and increasing line solidity denote higher Mach. A small increase in magnitude of the effect of the upstream shed vortex can be seen for the normal force and the bending moment, but for the hinge moment, an increase in Mach number actually reduces the coefficient magnitude. The effect is greatest when the upstream and downstream fins are pitched in opposite directions, suggesting that the leading edge of the downstream fin must be moved outside the position of the vortex core to create a meaningful Mach number influence. The relatively mild effect due to Mach number indicates that the increase in Mach number owing to boundary layer growth in the test section is not likely to be a significant factor in interpreting the data, when appropriately normalized.

Finally, the effect due to the axial spacing between fins may be examined. This value, G, is expressed as the distance between fin centers and is normalized by the fin root chord c. Three values were tested, G/c=1, 2, and 3 (where G/c=3 was used for the data in Figs. 5 and 6) and are shown in Fig. 7, where deepening color and increased line solidity denote larger G. As would be anticipated, a decrease to the fin spacing enhances the interaction effect because the vortex, whose strength decays with downstream distance, is stronger when it reaches the second fin. The magnitude of this effect is dependent upon each fin angle, likely due to the position of the leading edge of the downstream fin within the vortex.

A preliminary uncertainty analysis has been conducted for the aerodynamic data and shows that the absolute uncertainty is constant at about 0.2% of full-scale, including repeatability of the tunnel conditions, when normalized to obtain aerodynamic coefficients. Error bars, therefore, reach about twice the thickness of the lines plotted in Figs. 5-7, indicating that the uncertainties are consistently small and do not influence interpretation of the data presented.

Fin Vortex Velocimetry

PIV data were acquired with only a single fin placed into the wind tunnel because the presence of the downstream fin would partially occlude the images. It is assumed that the same vortex shed from the upstream fin would impinge upon the downstream fin were it present; i.e., that no upstream influence occurs from the downstream fin.

Mean velocity data are shown in Fig. 8 for M_∞=0.8 at four angles of attack of the single fin, α=0°, 2°, 5°, and 10°. The fin was mounted as far upstream in the wind tunnel as possible, therefore placing the PIV measurement location at a distance of x/c=4.18 from the trailing edge of the fin, which corresponds to G/c=4.68 (although aerodynamics are usually referenced to the fin's pivot point, vortices are commonly measured from the trailing edge of the surface from which they originate). In-plane velocities are displayed as vectors superposed upon a contour plot of the out-of-plane (streamwise) velocities. The

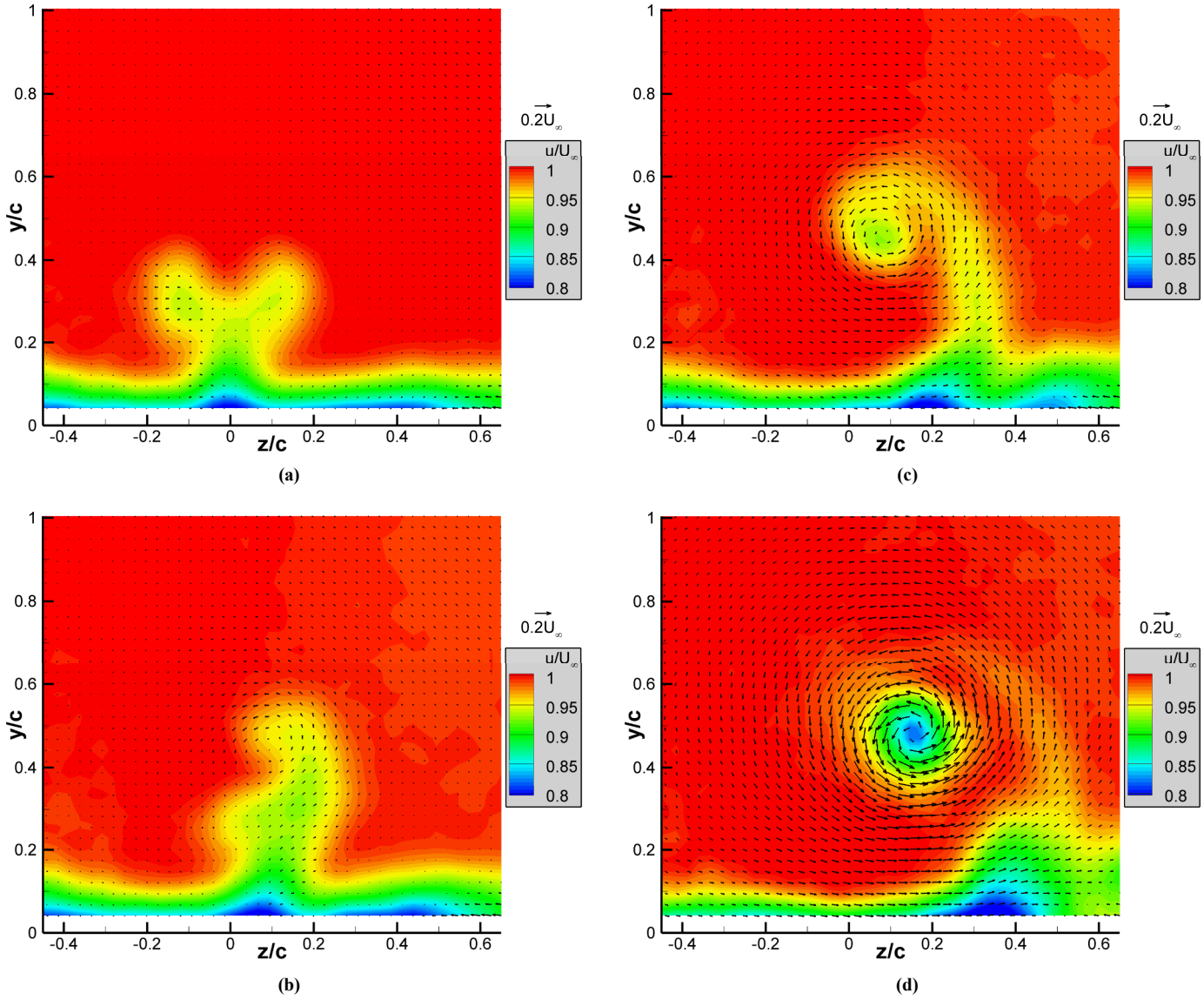

Figure 8: Mean velocity fields at M_∞=0.8 at a distance of x/c=4.18 from the trailing edge of the fin. (a) α=0°; (b) α=2°; (c) α=5°; (d) α=10°.

axes have been normalized to the fin root chord c and velocities by the freestream velocity as determined by the PIV data.

Figure 8 (in particular Figs. 8c and 8d) shows that the fin tip vortex is clearly visualized, both by the in-plane rotation and the out-of-plane streamwise velocity deficit. As the angle of attack is increased, the strength of the vortex increases markedly, seen in the magnitudes of both the in-plane velocity vectors and the streamwise velocity deficit. Although the α=0° case does not generate a vortex, a wake is still created, which would explain the small degree of aerodynamic interference observed in Figs 5-7 when the downstream fin is at large angle of attack. A close study of Fig. 8 shows that the vortex position moves laterally further from the centerline as α is increased, though naturally it remains at a height corresponding to the position of the fin tip. This lateral displacement exceeds the distance purely associated with the location of the fin trailing edge due to the fin cant.

The fin tip vortex itself is entirely analogous to the well-known wing tip vortices produced by aircraft, for which a wide range of velocimetry studies have been conducted (see, for example, [10-13]). The same characteristic structure is observed here, including the presence of a primary vortex core with a thin vortex sheet continuing to spiral around the core (in the present case, additionally lifting the wall boundary layer) and the prominence of axial flow within the vortex core.

The Mach number effect upon the fin tip vortex is shown in Fig. 9 at α=10°, excepting the M_∞=0.8 case that is given in Fig. 8d. As normalized here, no difference can be discerned between the four Mach numbers tested. Measurement of derived quantities such as the vortex circulation, centroid position, and size (not discussed in the present work for reasons of brevity) quantitatively support this observation. However, a subtle effect due to Mach number was detected by

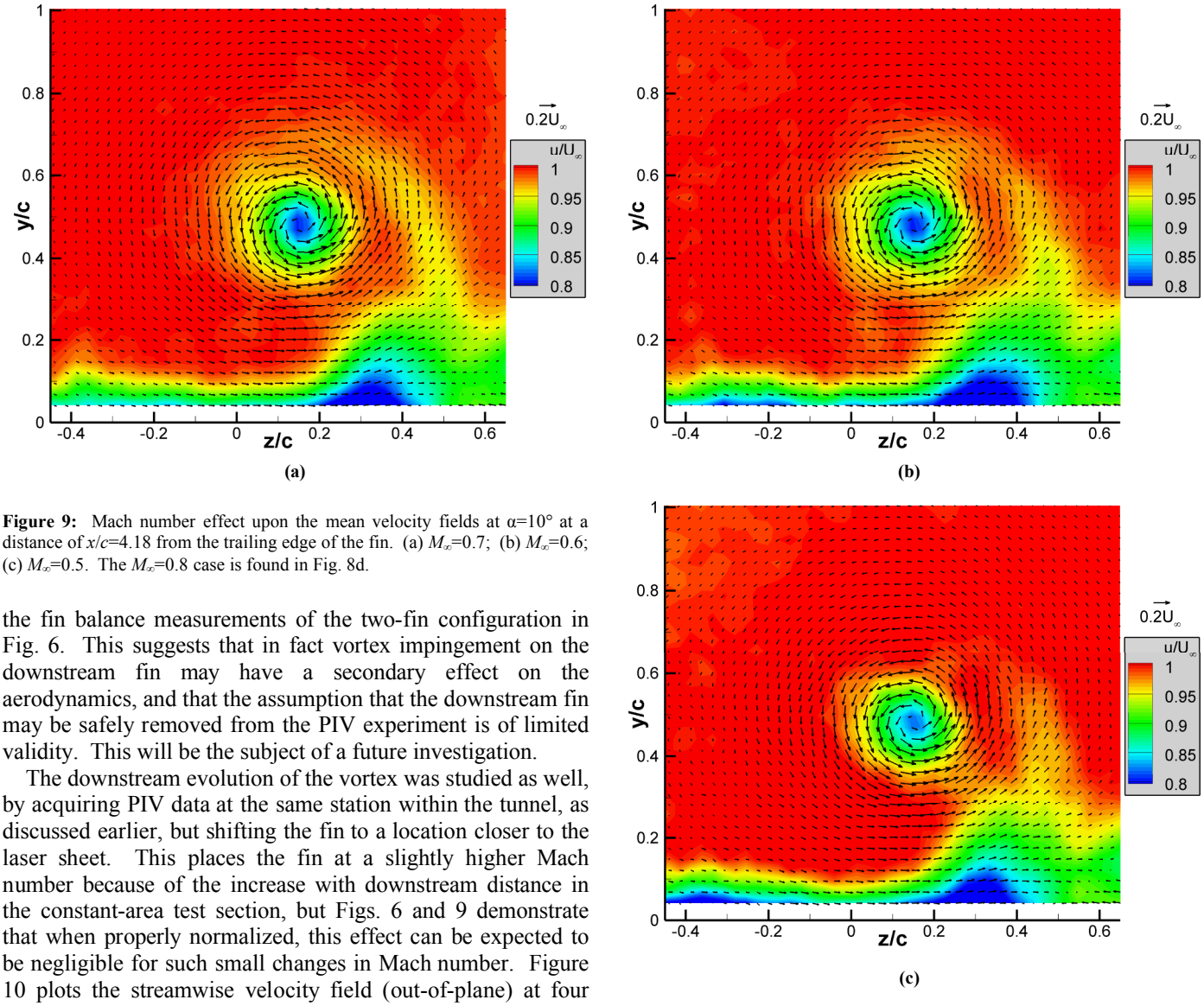

Figure 9: Mach number effect upon the mean velocity fields at α=10° at a distance of x/c=4.18 from the trailing edge of the fin. (a) M_∞=0.7; (b) M_∞=0.6; (c) M_∞=0.5. The M_∞=0.8 case is found in Fig. 8d.

the fin balance measurements of the two-fin configuration in Fig. 6. This suggests that in fact vortex impingement on the downstream fin may have a secondary effect on the aerodynamics, and that the assumption that the downstream fin may be safely removed from the PIV experiment is of limited validity. This will be the subject of a future investigation.

The downstream evolution of the vortex was studied as well, by acquiring PIV data at the same station within the tunnel, as discussed earlier, but shifting the fin to a location closer to the laser sheet. This places the fin at a slightly higher Mach number because of the increase with downstream distance in the constant-area test section, but Figs. 6 and 9 demonstrate that when properly normalized, this effect can be expected to be negligible for such small changes in Mach number. Figure 10 plots the streamwise velocity field (out-of-plane) at four downstream positions, showing the gradual decrease in the magnitude of the velocity deficit with downstream distance, accompanied by an apparent increase in vortex size. Though not visible in the figure, the magnitude of the in-plane velocities associated with the vortical rotation also decreases with downstream distance. Such measurements are useful for better understanding the underlying physics of the vortex shedding and for comparison with the aerodynamic effects of different fin spacing.

Preliminary uncertainty estimates of the PIV measurements indicate an uncertainty of about ±9 m/s, ±4 m/s, and ±6 m/s in the u, v, and w components, respectively, which equate to $0.03U_\infty$, $0.015U_\infty$, and $0.02U_\infty$, respectively, including repeatability of the tunnel conditions from one run to another. Additional wind tunnel runs were conducted in which the time between laser pulses was reduced from the standard value. Changing this parameter did not significantly alter the results, indicating that out-of-plane motion did not induce a bias error by selectively removing some particles from the PIV correlations.

Data Correlation

Given that the fin tip vortex visualized using PIV is responsible for the aerodynamic effects measured by the fin balance, a correlation between the two measurements would be anticipated. To examine this notion, the in-plane velocities from each mean PIV field were reduced to their derived vorticity field, from which the circulation Γ_x could be computed by integrating over a contour demarcating the approximate vortex boundary (the results discussed subsequently are found not to be dependent upon the contour definition). Figure 11 plots this value against ΔC_{NF}, the change in the normal force coefficient due to the interaction, as compared to the single fin value. As is clearly seen, a strong correlation is found. Since Fig. 8 shows that the position of the vortex shifts only mildly with a change in the upstream fin angle, it is logical that the vortex strength would be the dominant parameter driving the interaction. Data points are shown just for the PIV measurements at x/c=2.18, equivalent to G/c=2.68, and are plotted against ΔC_{NF} values interpolated

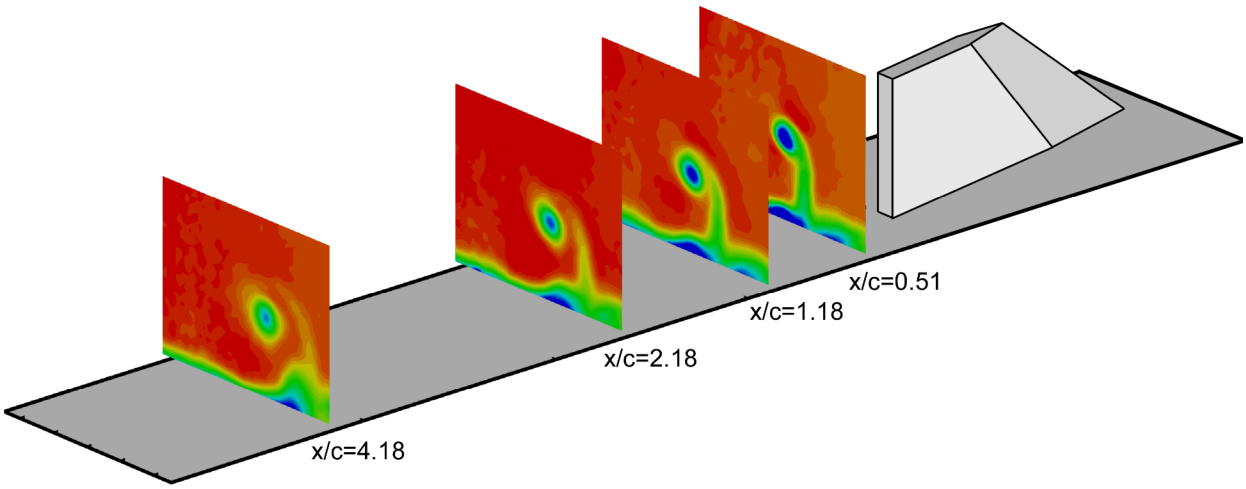

Figure 10: Mean streamwise velocity field (out-of-plane) at four downstream locations for M_∞=0.8 and α=10°.

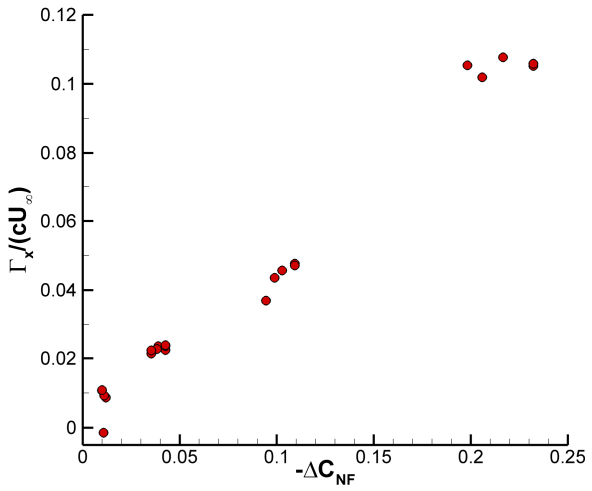

Figure 11: Correlation of vortex circulation derived from the PIV velocity field with the change in the normal force coefficient due to the interaction. Data shown at x/c=2.18.

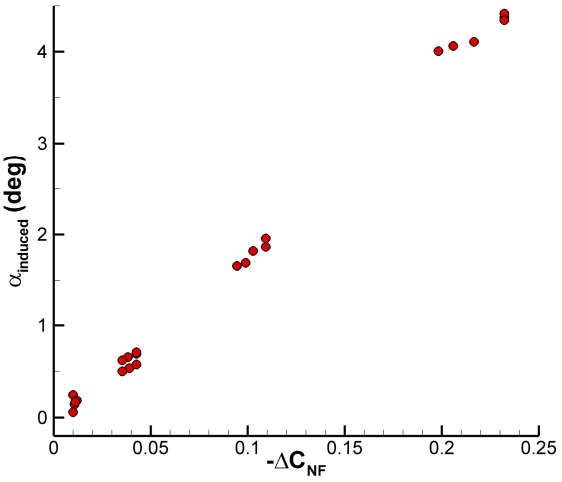

Figure 12: Correlation of the angle of attack upon a downstream fin induced by the vortex rotation with the change in the normal force coefficient due to the interaction. Data shown at x/c=2.18.

from the balance data of G/c=2 and 3. All Mach numbers and fin angles are plotted together. Results are similar when plotting the other PIV measurement planes against the nearest balance measurements. Results also are similar using ΔC_{BM} or ΔC_{HM} instead.

Because the vortex circulation is a quantity integrated from the velocity field, this suggests that a more fundamental relationship with the aerodynamic properties can be found in the velocities generated by the fin tip vortex. This possibility is examined by extracting from each PIV field the mean velocity vector along the fin span as if the downstream fin had been installed at the laser sheet location. From this velocity vector, the induced angle of attack upon the fin, $\alpha_{induced}$, may be calculated. This value is plotted against ΔC_{NF} in Fig. 12 for the same downstream station as Fig. 11, x/c=2.18. Again, a clear correlation is evident, and similar results are found at the other laser sheet locations or instead using ΔC_{BM} or ΔC_{HM}. These results are consistent with a previous study of the aerodynamic origins of jet/fin interaction, in which the vortices produced by the interaction of the exhausting jet with the freestream create an induced angle of attack on a downstream fin to alter its roll torque [14].

Conclusions and Future Work

To initiate a research program into fin tip vortices and their aerodynamic influence upon downstream control surfaces, a sub-scale experiment has been constructed using fins mounted on one test section wall of a transonic wind tunnel. Data are collected using two primary diagnostics, a fin balance mounted on the downstream fin to measure the aerodynamic forces of the interaction, and stereoscopic Particle Image Velocimetry (PIV) to measure the properties of the vortex responsible for the interaction.

The fin balance data show that the aerodynamic response of the downstream fin essentially is shifted above or below the baseline single-fin data dependent upon the angle of attack of the upstream fin. Freestream Mach number and the spacing between fins have secondary effects. The fin vortex

velocimetry shows that the vortex strength increases markedly with upstream fin angle of attack, though even an uncanted fin generates a noticeable wake. No effect due to Mach number can be discerned in the normalized data, but data taken at progressively further stations following the fin trailing edge show the decay in vortex strength with downstream distance. Correlations between the force data and the velocimetry suggest that the interaction is fundamentally a result of the angle of attack induced upon the downstream fin by the vortex shed from the upstream fin tip.

As the current project advances, enhancements will be made to the PIV configuration to improve the spatial resolution, reduce the measurement uncertainty, and acquire datasets sufficiently large to determine turbulence quantities. In addition, much more analysis than that presented here is possible, and further measurements will explore the role of vortex impingement on the downstream fin in the aerodynamic interaction. Concurrently, fin balance measurements in a porous-wall transonic test section with a half-body configuration will examine the interaction properties very near Mach 1. This approach will seek nonlinear behavior in the transonic regime that may be particularly difficult to predict, an investigation motivated in part by the nearly chaotic effects witnessed in a jet/fin interaction experiment [15].

These data will enhance our understanding of fin wake interactions to aid in the design of future flight vehicles, as well as directly providing measurements for the validation of computational models.

ACKNOWLEDGMENTS

The authors would like to thank B. Hassan, W. L. Oberkampf, J. L. Payne, and W. P. Wolfe, all of Sandia National Laboratories for their insightful advice.

This work is supported by Sandia National Laboratories and the United States Department of Energy. Sandia is a multiprogram laboratory operated by Sandia Corporation, a Lockheed Martin Company, for the United States Department of Energy's National Nuclear Security Administration under Contract DE-AC04-94AL85000.

REFERENCES

[1] Blake, W. B., "Missile DATCOM: User's Manual – 1997 Fortran 90 Revision," U.S. Air Force Research Lab/Air Vehicles Directorate, Wright-Patterson Air Force Base, OH, 1998.

[2] Dillenius, M. F. E., Lesieutre, D. J., Hegedus, M. C., Perkins, S. C. Jr., Love, J. F., and Lesieutre, T. O., "Engineering-, Intermediate-, and High-Level Aerodynamic Prediction Methods and Applications," *Journal of Spacecraft and Rockets*, Vol. 36, No. 5, pp. 609-620, 1999.

[3] Mikhail, A. G., "Assessment of Two Fast Aerodynamic Codes for Guided Projectiles," *Journal of Spacecraft*, Vol. 24, No. 4, pp. 303-310, 1987.

[4] Smith, E. H., Hebbar, S. K., and Platzer, M. F., "Aerodynamic Characteristics of a Canard-Controlled Missile at High Angles of Attack," *Journal of Spacecraft and Rockets*, Vol. 31, No. 5, pp. 766-772, 1994.

[5] Sooy, T. J., and Schmidt, R. Z., "Aerodynamic Predictions, Comparisons, and Validations Using Missile DATCOM (97) and Aeroprediction 98 (AP98)," *Journal of Spacecraft and Rockets*, Vol. 42, No. 2, pp. 257-265, 2005.

[6] Samimy, M., and Lele, S. K., "Motion of Particles with Inertia in a Compressible Free Shear Layer," *Physics of Fluids A*, Vol. 3, No. 8, pp. 1915-1923, 1991.

[7] Melling, A., "Tracer Particles and Seeding for Particle Image Velocimetry," *Measurement Science and Technology*, Vol. 8, No. 12, pp. 1406-1416, 1997.

[8] Soloff, S. M., Adrian, R. J., and Liu, Z-C, "Distortion Compensation for Generalized Stereoscopic Particle Image Velocimetry," *Measurement Science and Technology*, Vol. 8, No. 12, pp. 1441-1454, 1997.

[9] Beresh, S. J., Henfling, J. F., Erven, R. J., and Spillers, R. W., "Penetration of a Transverse Supersonic Jet into a Subsonic Compressible Crossflow," *AIAA Journal*, Vol. 43, No. 2, pp. 379-389, 2005.

[10] McCormick, B. W., Tangler, J. L., and Sherrieb, H. E., "Structure of Trailing Vortices," *Journal of Aircraft*, Vol. 5, No. 3, pp. 260-267, 1968.

[11] Hoeijmakers, H. W. M., "Vortex Wakes in Aerodynamics," *Characterization and Modification of Wakes from Lifting Vehicles in Fluid*, AGARD CP-584, 1996.

[12] Devenport, W. J., Rife, M. C., Liapis, S. I., and Follin, G. J., "The Structure and Development of a Wing-Tip Vortex," *Journal of Fluid Mechanics*, Vol. 312, pp. 67-106, 1996.

[13] Ozger, E., Schell, I., and Jacob, D., "On the Structure and Attenuation of an Aircraft Wake," *Journal of Aircraft*, Vol. 38, No. 5, pp. 878-887, 2001.

[14] Beresh, S. J., Heineck, J. T., Walker, S. M., Schairer, E. T., and Yaste, D. M., "Planar Velocimetry of Jet/Fin Interaction on a Full-Scale Flight Vehicle Configuration," forthcoming in *AIAA Journal*.

[15] Peterson, C. W., Wolfe, W. P., and Payne, J. L. "Experiments and Computations of Roll Torque Induced by Vortex-Fin Interaction," AIAA Paper 2004-1069, January 2004.